BMC Pulmonary Medicine

RESEARCH

Open Access

Changes in lung mechanics and ventilation-perfusion match: comparison of pulmonary air- and thromboembolism in rats

József Tolnai[1], Bence Ballók[1], Roberta Südy[2], Álmos Schranc[2], Gabriella Varga[3], Barna Babik[4], Gergely H. Fodor[1] and Ferenc Peták[1*]

Abstract

Background Pulmonary air embolism (AE) and thromboembolism lead to severe ventilation-perfusion defects. The spatial distribution of pulmonary perfusion dysfunctions differs substantially in the two pulmonary embolism pathologies, and the effects on respiratory mechanics, gas exchange, and ventilation-perfusion match have not been compared within a study. Therefore, we compared changes in indices reflecting airway and respiratory tissue mechanics, gas exchange, and capnography when pulmonary embolism was induced by venous injection of air as a model of gas embolism or by clamping the main pulmonary artery to mimic severe thromboembolism.

Methods Anesthetized and mechanically ventilated rats ($n=9$) were measured under baseline conditions after inducing pulmonary AE by injecting 0.1 mL air into the femoral vein and after occluding the left pulmonary artery (LPAO). Changes in mechanical parameters were assessed by forced oscillations to measure airway resistance, lung tissue damping, and elastance. The arterial partial pressures of oxygen (PaO_2) and carbon dioxide ($PaCO_2$) were determined by blood gas analyses. Gas exchange indices were also assessed by measuring end-tidal CO_2 concentration ($ETCO_2$), shape factors, and dead space parameters by volumetric capnography.

Results In the presence of a uniform decrease in $ETCO_2$ in the two embolism models, marked elevations in the bronchial tone and compromised lung tissue mechanics were noted after LPAO, whereas AE did not affect lung mechanics. Conversely, only AE deteriorated PaO_2, and $PaCO_2$, while LPAO did not affect these outcomes. Neither AE nor LPAO caused changes in the anatomical or physiological dead space, while both embolism models resulted in elevated alveolar dead space indices incorporating intrapulmonary shunting.

Conclusions Our findings indicate that severe focal hypocapnia following LPAO triggers bronchoconstriction redirecting airflow to well-perfused lung areas, thereby maintaining normal oxygenation, and the CO_2 elimination ability of the lungs. However, hypocapnia in diffuse pulmonary perfusion after AE may not reach the threshold level to induce lung mechanical changes; thus, the compensatory mechanisms to match ventilation to perfusion are activated less effectively.

Keywords Pulmonary air embolism, Pulmonary artery occlusion, Respiratory mechanics, Arterial blood gas parameters, Volumetric capnography, Ventilation-perfusion mismatch

*Correspondence:
Ferenc Peták
petak.ferenc@med.u-szeged.hu
Full list of author information is available at the end of the article

Background

Pulmonary embolism is a common adverse cardiovascular event and can lead to severe gas exchange and circulatory consequences [1]. This life-threatening condition can occur when air or other gases enter the pulmonary circulation, which commonly occurs following lung trauma, as a complication of childbirth, or during surgical interventions [2], scuba diving, or flying [3]. Another form of pulmonary embolism occurs when the pulmonary vessels are occluded by a solid blood clot or other bodily substance, such as following deep venous thrombi or in cancer-associated thrombosis [1, 4].

Although both gas- and thromboembolism compromise pulmonary blood flow, these disorders differ substantially, particularly in the regional distribution of pulmonary perfusion defects. Gas bubbles in the venous blood undergo turbulent mixing and disruption in the right ventricle, mainly leading to gravitation-dependent diffuse pulmonary hypoperfusion [5–7]. Conversely, the spatial distribution of thromboembolism is more focal and mainly affects distinct lung areas [8–10]. These fundamental differences in the spatial distribution of the lung perfusion defects may affect the adverse changes in respiratory mechanics, gas exchange, and ventilation-perfusion match. Thus, major differences can be anticipated in the outcomes of these two forms of embolism. Nevertheless, the effects of pulmonary perfusion defects in models of thrombo- or gas embolism have not been compared in a study.

Therefore, we aimed to compare changes in indices reflecting airway and respiratory tissue mechanics, gas exchange, and capnography parameters when lung embolism is induced by venous injection of air bubbles as a model of gas embolism or by clamping the main pulmonary artery to mimic severe thromboembolism.

Methods

Ethical statement

This experimental protocol was included in a research project approved by the National Food Chain Safety and Animal Health Directorate of Csongrád County, Hungary (no. XXXII./2096/2018) on September 24, 2018. The experimental procedures were performed according to the guidelines of the Scientific Committee of Animal Experimentation of the Hungarian Academy of Sciences (updated Law and Regulations on Animal Protection: 40/2013. [II. 14.], Government of Hungary) and European Union Directive 2010/63/EU on the protection of animals used for scientific purposes. All methods are reported in accordance with ARRIVE guidelines for the reporting of animal experiments [11].

Animal preparation

Nine male Wistar rats (362 ± 25 g) were anesthetized by the intraperitoneal injection of sodium pentobarbital (45 mg/kg; Sigma-Aldrich, Budapest, Hungary). The left femoral artery and vein were cannulated by 23 G catheters to administer medications, monitor blood pressure, and collect blood samples. Anesthesia was maintained with intravenous sodium pentobarbital (5 mg/kg) every 30 min, and muscle relaxation was obtained by neuromuscular blockade with repeated intravenous boluses of pipecuronium (0.2 mg/kg every 30 min; Arduan, Richter-Gedeon, Budapest, Hungary). The body temperature of the rats was maintained at 37 °C ± 0.5 °C throughout the experiment using a heating pad equipped with a rectal thermometer (model 507223F; Harvard Apparatus, Holliston, MA, USA).

The animals were tracheostomized after additional local anesthesia with subcutaneous lidocaine (2–4 mg/kg), and the trachea was cannulated with an 18 G uncuffed endotracheal tube. Volume-controlled mechanical ventilation with a tidal volume (VT) of 7 mL/kg and positive end-expiratory pressure (PEEP) of 5 cmH_2O was applied using a small animal ventilator (Model 683; Harvard Apparatus, South Natick, MA, USA). The ventilation frequency was set to 55–60 breaths/min to maintain an end-tidal CO_2 ($ETCO_2$) level within the normal range (35–45 mmHg). Midline thoracotomy was then performed to access the left pulmonary artery. The mean arterial pressure (MAP) and heart rate (HR) were monitored and recorded using a data collection and acquisition system (Powerlab 8/35 and Labchart, ADInstruments, Dunedin, New Zealand).

Measurement of airway and respiratory tissue mechanics

The mechanical parameters of the airway and respiratory tissues were determined by measuring the input impedance of the respiratory system (Zrs) using the wave-tube approach of the forced oscillation technique [12]. Briefly, the tracheal cannula was attached to a loudspeaker-in-box system, which generated a small-amplitude pseudorandom forcing signal (amplitudes < 1.5 cmH_2O with 23 non-integer multiple-frequency components in the range of 0.5–20.75 Hz) through a wave-tube (polyethylene; length, 100 cm; internal diameter, 2 mm). During these measurements, ventilation was briefly suspended (8 s) at end-expiration, and the oscillatory pressures were measured with two identical miniature differential pressure transducers (Honeywell Differential Pressure Sensor model 24PCEFA6D; Honeywell, Charlotte, NC, USA) at the loudspeaker and tracheal ends of the wave-tube. After a minimum of four technically acceptable measurements in each protocol phase, Zrs values were calculated as the

load impedance of the wave-tube [12]. The mechanical properties of the respiratory system were obtained by fitting the well-established and validated constant phase model to the ensemble-averaged Zrs spectra (16). This model comprised frequency-independent airway resistance (Raw) and airway inertance in series with a viscoelastic constant phase tissue unit that includes tissue elastance (H) and tissue damping (G) [13]. Hysteresivity, reflecting the coupling of the resistive and elastic properties within the viscoelastic respiratory tissues, was calculated as $\eta = G/H$ [14].

Blood gas analyses

Samples of 0.15 mL arterial blood were collected for blood gas analyses, from which the arterial partial pressures of oxygen (PaO_2) and carbon dioxide ($PaCO_2$) were determined using a point-of-care blood analyzer system (Epoc Reader and Host; Epocal, Inc., Ottawa, ON, Canada).

Recording and analyses of volumetric capnograms

The partial pressure of carbon dioxide (PCO_2) in expired gas and ventilation airflow (V') were simultaneously recorded using a rodent sidestream volumetric capnograph (Harvard Capnograph Type 340 for small rodents) at a sampling frequency of 256 Hz. Volumetric capnogram curves were generated for each expiratory cycle from the PCO_2 tracing and the volume signals obtained by integrating the corresponding V' data. The capnogram phase boundaries were determined, and the shape factors were calculated based on previously described concepts [15, 16]. Briefly, the inflection point of phase 2 was determined as the maximum of the first derivative of the volumetric capnogram curve, and the phase 2 slope (S2V) was measured as the rate of change of PCO_2 around this inflection point. The start and end points of phase 2, which reflect the mixed emptying of airway-alveolar spaces, were identified as the maxima of the third derivative before and after this inflection point in both the time and volumetric domains. The phase 3 capnogram slope (S3V), reflecting the dynamics of the alveolar gas compartment emptying, was determined by fitting a linear regression line to the middle third of phase 3. Normalized phase 2 (Sn2V) and 3 (Sn3V) slopes were calculated by dividing S2V and S3V by the respective $ETCO_2$ values. This normalization allows a more objective comparison of changes in the capnogram shape due to changes in $ETCO_2$, such as observed in the embolism models used in the present study [17–19].

Volumetric capnography also enables the calculation of Fowler's anatomic dead space (VDF), Bohr's physiological dead space (VDB), and Enghoff's modified physiological dead space (VDE). VDF was defined as the exhaled gas volume until the inflection point in phase 2 [20]. VDB was calculated as [21]:

$$VDB/VT = \left(PACO_2 - P\bar{E}CO_2\right)/PACO_2$$

where the mean alveolar partial pressure of CO_2 ($PACO_2$) was defined as the CO_2 concentration at the midpoint of phase 3 in the volumetric capnography curve, and the mixed expired CO_2 partial pressure ($P\bar{E}CO_2$) was estimated by dividing the integrated capnogram curve by VT in each expiratory cycle.

VDE, which also comprises nonventilated but perfused alveoli, also known as intrapulmonary shunting, was obtained as follows [22, 23]:

$$VDE/VT = \left(PaCO_2 - P\bar{E}CO_2\right)/PaCO_2$$

where $PaCO_2$ is the partial pressure of CO_2 in an arterial blood sample.

The alveolar dead space fraction (AVDSf) was also determined as $(PaCO_2\text{-}ETCO_2)/PaCO_2$ [24].

Pilot experiments

In these preliminary experiments, 4 and 2 animals were used to examine the hemodynamic and respiratory responses to air injections of 0.2 ml and 0.15 ml, respectively. However, the responses observed in these pilot rats were excessively severe, resulting in lethal outcomes for 3 rats. These preliminary findings were the basis of the decision to use a 0.1 ml air bubble in the main protocol group.

Study protocol

Following anesthesia induction and surgical preparations, including the thoracotomy, the rats were ventilated as described above with a PEEP of 5 cmH_2O throughout the study. After stabilizing vital parameters, a lung recruitment maneuver was performed by closing the expiratory limb of the ventilator tubing until the next expiration to standardize lung volume history. Baseline data were collected 1–2 minutes later by recording capnograph curves and forced oscillation data, along with blood gas analyses of arterial blood samples. Pulmonary air embolism (AE) was then induced by injecting 0.1 mL of air (0.5% of total blood volume) mixed with 0.9 mL of saline into the femoral vein while continuously monitoring the changes in systemic hemodynamics and the capnogram. This injected air volume was titrated in pilot experiments to exert similar changes in $ETCO_2$ compared to those observed after unilateral pulmonary artery occlusion, yielding comparable gas exchange defects assessed in the expired gas (*see above*). When a peak decrease in $ETCO_2$ was observed (10–15 seconds after the air injection), an additional data set was recorded (condition AE).

The effects of AE on systemic hemodynamics and gas exchange parameters lasted approximately 2–4 minutes and then returned to the normal range after approximately 5 minutes, as verified by the continuous monitoring of relevant vital signs. After a 10–15-min stabilization period, the left pulmonary artery was clamped using a small-sized surgical clip, and a third data set, including capnography, forced oscillations, and blood gas analyses, was collected under this condition, i.e. during left pulmonary artery occlusion (LPAO).

Statistical analysis

Data are presented as the median with interquartile ranges in each boxplot chart. The Shapiro–Wilk test was used to evaluate the data distributions for normality. For each parameter studied, one-way repeated-measures ANOVA with Holm–Šidák post hoc tests was applied to assess significant differences between the results obtained in the protocol phases. Statistical analyses were performed with the SigmaPlot software package (Version 14, Systat Software, Inc., Chicago, IL, USA).

Since changes in lung tissue stiffness were anticipated after embolism, H was considered the primary outcome variable for estimating sample size using one-way repeated-measures ANOVA, with an effect size (f) of 0.4, power of 0.8, and significance level of 0.05. This analysis performed using G*Power (version 3.1.9.7, Universität Düsseldorf, Germany) indicated that at least nine animals were required to detect a 15% significant difference in the primary outcome when considering the previously observed variability [25]. Statistical analyses were performed at a significance level of $P < 0.05$.

Results

The mechanical parameters of the respiratory system under baseline conditions and following induction of pulmonary embolism by two different mechanisms are shown in Fig. 1. No significant changes in these parameters were observed after AE. In contrast, significant

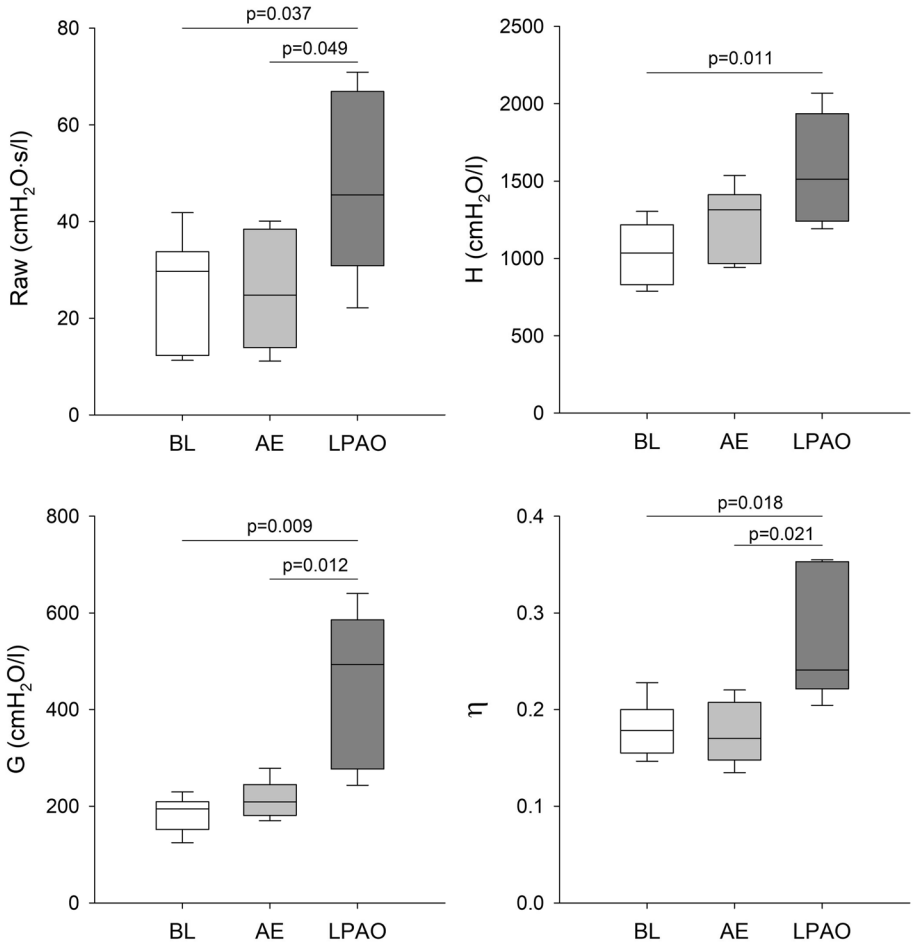

Fig. 1 Airway and respiratory tissue mechanical parameters at baseline (BL), following air embolism (AE), and after left pulmonary artery occlusion (LPAO). Raw: airway resistance, H: tissue elastance, G: tissue damping, η: tissue hysteresivity (G/H)

increases in all parameters reflecting airway (Raw) and respiratory tissue mechanics (H, G, and η) were obtained after clamping the left pulmonary artery compared to baseline values ($P<0.05$ for all). Significant differences in Raw, G, and η were observed between the two forms of embolism ($P<0.05$ for all), while there was a trend toward a significant difference in H ($P=0.1$).

Figure 2 summarizes $ETCO_2$, the $PaCO_2$-$ETCO_2$ gradient, and the arterial blood gas parameters under the baseline condition and following the induction of embolism by the two different mechanisms. In accordance with our experimental approach to induce comparable gas exchange defects assessed in the expired CO_2 concentration, the significant decreases in $ETCO_2$ did not differ between the two embolism models ($p<0.001$ vs. baseline for both). Furthermore, increases in $PaCO_2$-$ETCO_2$ of comparable magnitude were observed in both embolism models ($P<0.05$ vs. baseline for both). A significant decrease in PaO_2 and a significant increase in $PaCO_2$ were observed following AE ($P<0.001$ for both). However, these parameters were not significantly affected by LPAO, resulting in significant differences in PaO_2 and $PaCO_2$ between the two forms of pulmonary embolism ($P<0.001$ for both). There was a strong tendency for an increase in the arterial lactate level, with increasing from the baseline value of 2.6 ± 0.8 mmol/L to 3.6 ± 1.3 and 4.3 ± 1.8 mmol/L after AE and LPAO, respectively ($p=0.056$).

Figure 3 shows shape factors representing the normalized phase 2 and phase 3 slopes obtained by volumetric capnography. No significant change in Sn2V was observed after either form of embolism. In contrast, significant increases in Sn3V were evidenced following LPAO compared to baseline and after AE ($P<0.05$ for both).

Changes in dead space indices at different protocol stages are shown in Fig. 4. There were no significant changes in VDF or VDB following either form of embolism. However, a significant increase in the VDE dead space fraction was observed following AE and LPAO

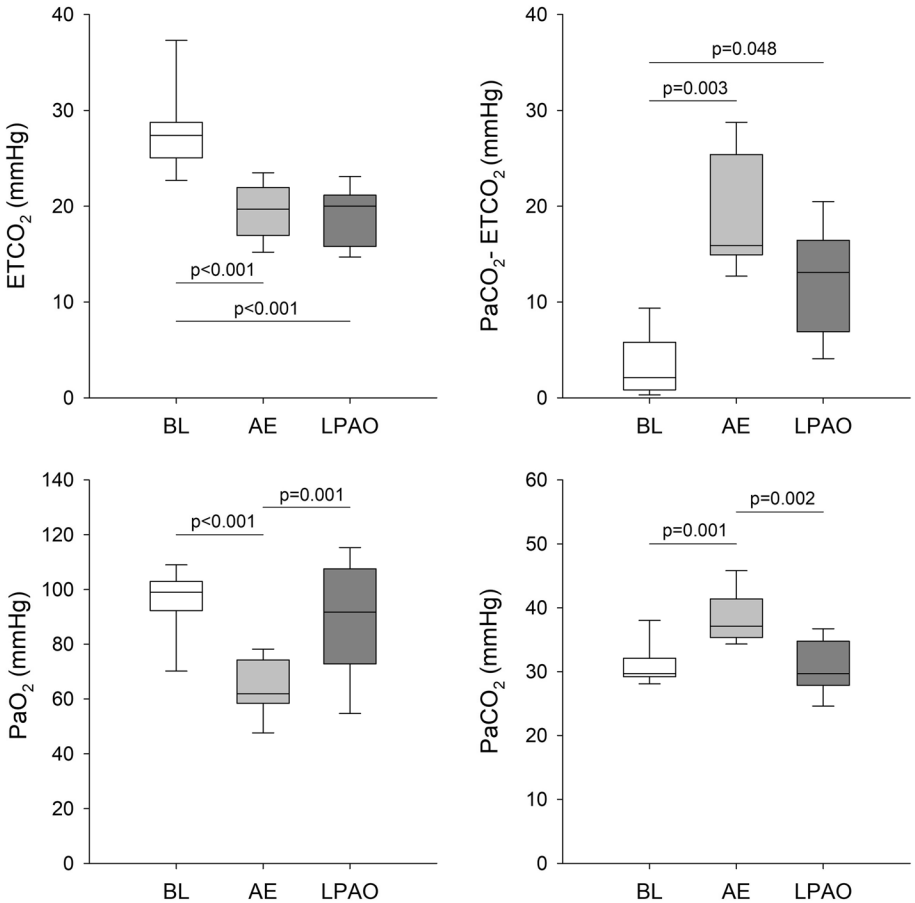

Fig. 2 Arterial blood gas parameters and related capnogram indices obtained at baseline (BL), following air embolism (AE), and after left pulmonary artery occlusion (LPAO).$ETCO_2$: end-tidal carbon dioxide, $PaCO_2$-$ETCO_2$: arterial to the end-tidal CO_2 pressure gradient, PaO_2: arterial partial pressure of oxygen, $PaCO_2$: arterial partial pressure of carbon dioxide

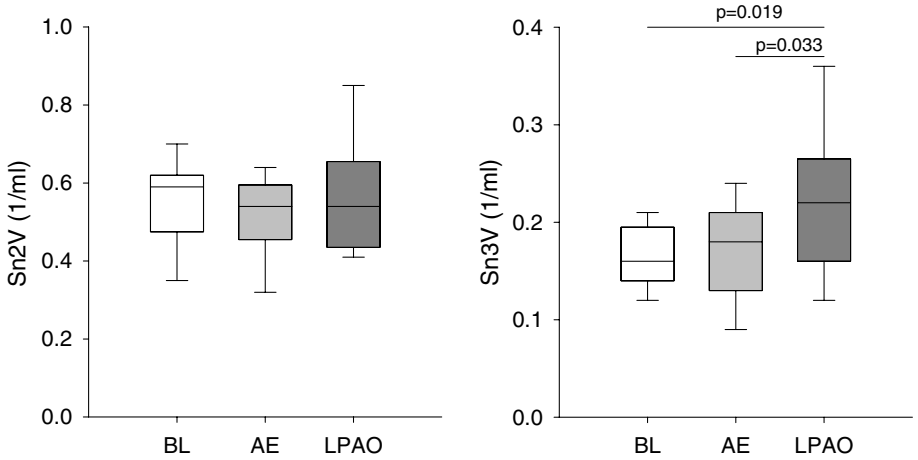

Fig. 3 Phase 2 and 3 slopes of the volumetric capnogram normalized to the end-tidal CO_2 concentration obtained at baseline (BL), following air embolism (AE), and after left pulmonary artery occlusion (LPAO)

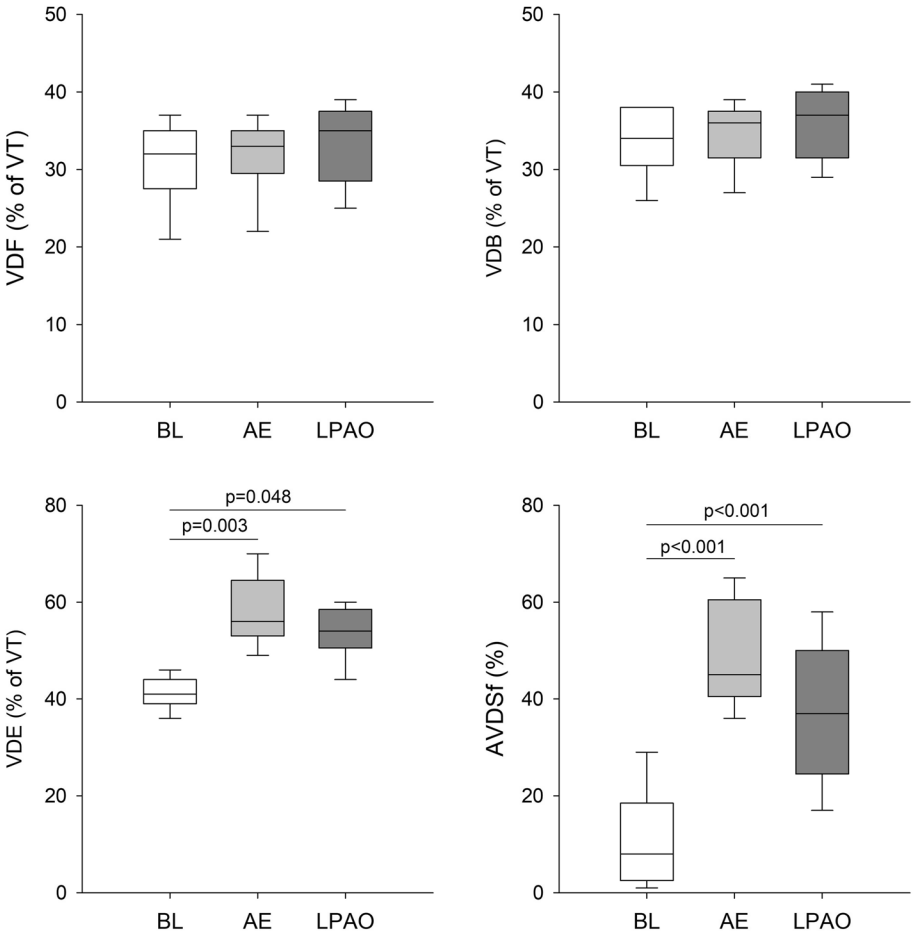

Fig. 4 Fowler anatomical (VDF), Bohr (VDB), and Enghoff (VDE) physiological dead spaces, and alveolar dead space fraction (AVDSf) expressed as a percentage of tidal volume (% of VT) obtained at baseline (BL), following air embolism (AE), and after left pulmonary artery occlusion (LPAO)

($P=0.003$ and $P<0.05$, respectively). A significant increase in AVDSf compared to the baseline condition was also observed following both forms of embolism ($P<0.001$ for both), with a trend toward increased AVDSf following AE compared to LPAO ($P=0.063$).

Table 1 demonstrates the changes in the systemic hemodynamics before, during, and after the embolic insults. AE and LPAO induced significant transient decreases in MAP and HR ($p<0.001$, for all). Complete recoveries of MAP and HR were observed after AE with no significant difference compared to the values obtained before the interventions.

Discussion

The present study revealed fundamental differences between models of pulmonary embolisms, although comparable decreases in the expired carbon dioxide concentration were induced by the gas- and thromboembolic models. Unilateral pulmonary arterial occlusion caused marked elevations in the bronchial tone and compromised lung tissue mechanics, whereas air embolism did not affect lung mechanics. In contrast with these lung mechanical changes, air embolism was the only insult that caused significant deteriorations in the arterial blood gas parameters, while partial pressures of oxygen and carbon dioxide in the arterial blood were unaffected by left pulmonary artery occlusion. No changes in anatomical (Fowler) or physiological dead space reflecting ventilated but poorly perfused lung areas (Bohr) were observed in either embolism model. Conversely, both air embolism and unilateral pulmonary artery occlusion resulted in elevated alveolar dead space indices that indicate intrapulmonary shunting (Enghoff and AVDSf).

The main finding of the present study was that distinct lung mechanical responses developed in response to the different models of lung embolism, even in the presence of similarly deteriorated $ETCO_2$ levels. In contrast to the lack of changes in lung mechanics following AE, marked bronchoconstriction developed in response to LPAO (Fig. 1). This finding can be explained by the ability of the CO_2 content of the intrapulmonary gas to modulate the airway smooth muscle tone, resulting in severe bronchospasm below a threshold partial pressure of CO_2 of approximately 10 mmHg [26]. Reaching this threshold CO_2 concentration in the ischemic left lung during LPAO explains the elevations in airway resistance. The magnitude of the overall increase in the airway resistance was blunted by the intact right lung, which was probably somewhat overinflated. Conversely, the diffuse pulmonary hypoperfusion that developed after AE was likely to cause a moderate and relatively evenly distributed hypocapnia in the bronchoalveolar system, in which the threshold concentration to trigger a bronchial smooth muscle contraction was not reached [26].

These differences in the airway responses between AE and LPAO were associated with distinct changes in the forced oscillatory parameters reflecting respiratory tissue damping (G) and stiffness (H). The excessive increase in G over those in H indicates the development of ventilation heterogeneities [27]. As this pattern of change was observed only after LPAO, the impairment in respiratory tissue mechanics indicates that considerable ventilation inhomogeneity developed after LPAO due to uneven lung ventilation resulting from the additive effects of volume loss in the left lung and overdistension of the right lung. The presence of this phenomenon was confirmed by the elevations in mechanical and capnography parameters sensitive to ventilation heterogeneities (η and Sn3V).

Changes in blood gas parameters notably differed between the two embolism models, with significant deteriorations observed only after a diffuse pulmonary perfusion defect generated by AE (Fig. 2). In agreement with previous findings [28–30], acute AE led to the development of hypoxia and hypercapnia. The adverse gas exchange defects were reflected in the alveolo-end-tidal CO_2 gradient (Fig. 2) and in the marked elevations in VDE and AVDSf (Fig. 4). Since VDE and AVDSf incorporate poorly ventilated but perfused alveoli with low V/Q [31], increased intrapulmonary shunting may be responsible for this finding as a consequence of a perfusion redistribution [30]. Interestingly, blood gas parameters were unaffected by LPAO despite concomitant increases in capnography parameters reflecting intrapulmonary low V/Q areas and shunting ($PaCO_2$-$ETCO_2$ in Fig. 2 and VDE and AVDSf in Fig. 3) and in the airway and respiratory tissue mechanics (Fig. 1). The absence of changes in PaO_2 following LPAO agrees with previous results demonstrating that oxygenation can remain normal following

Table 1 Mean arterial pressure (MAP) and heart rate (HR) expressed as mean ± SD obtained before air embolism (Before AE), at the peak response following AE, and 2 minutes later. Values are also reported immediately before the left pulmonary artery occlusion (LPAO), at the peak response after LPAO, and 2 minutes after release of the left pulmonary artery. *: $p<0.001$ vs. BL, #: $p<0.001$ vs. AE, $: $p=0.013$ vs. AE

	Before AE	AE	2 mins after AE	Before LPAO	LPAO	2 mins after LPAO
MAP (mmHg)	116 ± 11	64 ± 21*	110 ± 9	125 ± 4	30 ± 10*#	108 ± 12
HR (BPM)	490 ± 57	352 ± 48*	474 ± 69	473 ± 24	215 ± 46*$	463 ± 24

acute pulmonary thromboembolism [32, 33]. This finding is likely attributable to the unaffected right lung being able to maintain blood gas parameters within the normal range due to increased VT in response to hypocapnic bronchoconstriction in the ischemic left lung [34].

No change in VDF was observed after inducing lung embolism using air bubbles or unilateral pulmonary vascular ischemia (Fig. 3). As VDF reflects the amount of gas in the conducting airways [20], this finding demonstrates that there was no change in the anatomical dead space fraction following either intervention. While severe bronchoconstriction in the hypocapnic left lung may yield a unilateral reduction in apparent anatomic dead space [35], the redistribution of tidal volume to the right lung may have overinflated this compartment, thereby counterbalancing the anatomic dead space.

The lack of change in VDB after either form of embolism is worth noting (Fig. 3). Unilateral occlusion of the pulmonary artery is expected to result in nonperfused but well-ventilated lung regions. Furthermore, the development of a similar ventilation-perfusion mismatch is expected after introducing air into the pulmonary circulation. Accordingly, elevations in VDB can be anticipated in both models of embolism based on Riley's 3-compartment lung model, in which VDB reflects the amount of well-ventilated but poorly perfused alveolar compartments [36]. This seemingly controversial result can be explained by the complex pathophysiological processes initiated by the massive ventilation-perfusion mismatch after embolism. Development of severe bronchoconstriction in the hypocapnic left lung following LPAO can reach a degree where airflow redistribution from the left into the right lung results in a constant VDB. The presence of this mechanical defect after LPAO was confirmed by our forced oscillatory data demonstrating marked elevations in airway resistance (Fig. 1). The lack of change in VDB following AE may be attributable to the relatively small amount of air reaching the pulmonary circulation (6–8% of total intrapulmonary blood volume) that may have caused no major perfusion defects.

A methodological consideration of the present protocol is related to the protocol design, which focused on the acute consequences of pulmonary embolism. This approach allowed the comparison of two pulmonary circulatory insults in an animal model, thereby strengthening the statistical power and reducing the need for an excessive number of animals in accordance with the 3R principle. Indeed, complete recovery of monitored gas exchange ($ETCO_2$) and systemic circulatory parameters (MAP, HR) was observed between the interventions (Table 1), which suggests the lack of a carryover effect between the protocol stages. However, the generalization of our findings to prolonged pulmonary perfusion defects should be considered. An additional limitation of the present study is that volumetric capnography provides an overall picture about the V/Q matching for the entire lungs. Expanded use of imaging techniques, such as SPECT [37], K-edge subtraction [38], electric impedance tomography [39], or quantitative V/Q analysis by inert gas elimination [40] have the potential in forthcoming studies to further investigate the mechanisms by allowing regional assessments.

Conclusions

Marked differences in lung mechanical, gas-exchange, and capnography indices were observed following diffuse lung injury induced by the intravenous injection of air bubbles as a model of gas embolism or following clamping of the left pulmonary artery to mimic focal thromboembolism. Deteriorations in the lung mechanics reflecting the development of heterogeneous bronchoconstriction were observed after a focal ischemic insult in the pulmonary perfusion. However, the severity of hypocapnia did not reach the threshold level to alter the bronchial tone in any lung regions following a diffuse pulmonary perfusion defect subsequent to air embolism. In contrast with these lung mechanical changes, arterial blood gas parameters deteriorated following a diffuse pulmonary perfusion defect due to air embolisms, while focal perfusion defects due to pulmonary vascular occlusion triggered a compensatory respiratory mechanical response leading to airflow redistribution to lung areas with maintained perfusion, thereby maintaining normal oxygenation and CO_2 elimination. The findings that air and thromboembolism affect lung mechanics and gas exchange differently may have a relevance in tailoring respiratory support for patients.

Abbreviations

AE	Air embolism
ANOVA	Analysis of variance
ARRIVE	Animal research: reporting of in vivo experiments
AVDSf	Alveolar dead space fraction
$ETCO_2$	End-tidal carbon dioxide concentration
G	Tissue damping
H	Tissue elastance
HR	Heart rate
LPAO	Left pulmonary artery occlusion
MAP	Mean arterial pressure
PaO_2	Arterial partial pressures of oxygen
$PaCO_2$	Arterial partial pressures of carbon dioxide
$PACO_2$	Mean alveolar partial pressure of carbon dioxide
PCO_2	Partial pressure of carbon dioxide
PEEP	Positive end-expiratory pressure
$P\bar{E}CO_2$	Mixed expired CO_2 partial pressure
Raw	Airway resistance
S2V	Phase 2 slope of the volumetric capnogram
S3V	Phase 3 slope of the volumetric capnogram
Sn2V	Normalized phase 2 slope of the volumetric capnogram
Sn3V	Normalized phase 3 slope of the volumetric capnogram
V′	Ventilation airflow

VT	Tidal volume
VDB	Bohr's physiological dead space
VDE	Enghoff's modified physiological dead space
VDF	Fowler's anatomic dead space
Zrs	Input impedance of the respiratory system
η	Tissue hysteresivity

Acknowledgements
The authors thank Orsolya Ivánkovitsné Kiss for the excellent technical assistance.

Authors' contributions
J.T., G.H.F., and F.P. conceived and designed the research; J.T., G.H.F., R.S., Á.S., G.V., Bence. B. and F.P. performed the experiments; J.T., G.H.F., G.V., and F.P. analyzed the data; J.T., Barna B., and F.P. interpreted the results of the experiments; J.T., and F.P. prepared the figures; J.T. and F.P. drafted the manuscript; J.T., G.H.F., R.S., Á.S., G.V., Barna B., Bence B., and F.P. edited and revised the manuscript; all authors approved the final version of the manuscript.

Funding
Open access funding provided by University of Szeged. This work was supported by a Hungarian Basic Research Council Grant (OTKA-NKFIH K138032 and FK134274).

Availability of data and materials
The datasets used and/or analysed during the current study are available from the corresponding author on reasonable request.

Declarations

Ethics approval and consent to participate
All experimental protocols were approved by the National Food Chain Safety and Animal Health Directorate of Csongrád County, Hungary (no. XXXII./2096/2018) on September 24, 2018. All methods are reported in accordance with ARRIVE guidelines for the reporting of animal experiments.

Consent for publication
Not applicable.

Competing interests
The authors declare no competing interests.

Author details
[1]Department of Medical Physics and Informatics, University of Szeged, 9 Korányi fasor, Szeged H-6720, Hungary. [2]Unit for Anesthesiological Investigations, Department of Anesthesiology, Pharmacology, Intensive Care and Emergency Medicine, University of Geneva, 1 Rue Michel-Servet, 1206 Geneva, Switzerland. [3]Institute of Surgical Research, University of Szeged, 1 Pulz utca, Szeged H-6724, Hungary. [4]Department of Anesthesiology and Intensive Therapy, University of Szeged, 6 Semmelweis str., Szeged H-6725, Hungary.

Received: 23 August 2023 Accepted: 3 January 2024
Published online: 10 January 2024

References

1. Tarbox AK, Swaroop M. Pulmonary embolism. Int J Crit Illn Inj Sci. 2013;3(1):69–72.
2. Freund MC, Petersen J, Goder KC, Bunse T, Wiedermann F, Glodny B. Systemic air embolism during percutaneous core needle biopsy of the lung: frequency and risk factors. BMC Pulm Med. 2012;12:2.
3. Gordy S, Rowell S. Vascular air embolism. Int J Crit Illn Inj Sci. 2013;3(1):73–6.
4. Chen Z, Feng T, Wang M, Xu X, Wang Y, Li Y, Min L. Rare cause of repeated pulmonary embolism: a case of primary pleural squamous cell carcinoma and literature review. BMC Pulm Med. 2020;20(1):75.
5. Souders JE, Doshier JB, Polissar NL, Hlastala MP. Spatial distribution of venous gas emboli in the lungs. J Appl Physiol (1985). 1999;87(5):1937–47.
6. Calderon AJ, Fowlkes JB, Bull JL. Bubble splitting in bifurcating tubes: a model study of cardiovascular gas emboli transport. J Appl Physiol (1985). 2005;99(2):479–87.
7. Chang HK, Delaunois L, Boileau R, Martin RR. Redistribution of pulmonary blood flow during experimental air embolism. J Appl Physiol Respir Environ Exerc Physiol. 1981;51(1):211–7.
8. Atalay MK, Walle NL, Grand DJ, Mayo-Smith WW, Cronan JJ, Egglin TK. Scan length optimization for pulmonary embolism at CT angiography: analysis based on the three-dimensional spatial distribution of 370 emboli in 100 patients. Clin Radiol. 2011;66(5):405–11.
9. Tsang JY, Lamm WJ, Starr IR, Hlastala MP. Spatial pattern of ventilation-perfusion mismatch following acute pulmonary thromboembolism in pigs. J Appl Physiol (1985). 2005;98(5):1862–8.
10. Zhang J, Chen Y, Wang Z, Chen X, Liu Y, Liu M. Anatomic distribution of lower extremity deep venous thrombosis is associated with an increased risk of pulmonary embolism: a 10-year retrospective analysis. Front Cardiovasc Med. 2023;10:1154875.
11. Percie du Sert N, Hurst V, Ahluwalia A, Alam S, Avey MT, Baker M, Browne WJ, Clark A, Cuthill IC, Dirnagl U, et al. The ARRIVE guidelines 2.0: updated guidelines for reporting animal research. PLoS Biol. 2020;18(7):e3000410.
12. Petak F, Hantos Z, Adamicza A, Asztalos T, Sly PD. Methacholine-induced bronchoconstriction in rats: effects of intravenous vs. aerosol delivery. J Appl Physiol (1985). 1997;82(5):1479–87.
13. Hantos Z, Daroczy B, Suki B, Nagy S, Fredberg JJ. Input impedance and peripheral inhomogeneity of dog lungs. J Appl Physiol (1985). 1992;72(1):168–78.
14. Fredberg JJ, Stamenovic D. On the imperfect elasticity of lung tissue. J Appl Physiol (1985). 1989;67(6):2408–19.
15. Tusman G, Scandurra A, Bohm SH, Suarez-Sipmann F, Clara F. Model fitting of volumetric capnograms improves calculations of airway dead space and slope of phase III. J Clin Monit Comput. 2009;23(4):197–206.
16. Tolnai J, Fodor GH, Babik B, Dos Santos RA, Bayat S, Petak F, Habre W. Volumetric but not time capnography detects ventilation/perfusion mismatch in injured rabbit lung. Front Physiol. 2018;9:1805.
17. Tusman G, Areta M, Climente C, Plit R, Suarez-Sipmann F, Rodriguez-Nieto MJ, Peces-Barba G, Turchetto E, Bohm SH. Effect of pulmonary perfusion on the slopes of single-breath test of CO2. J Appl Physiol (1985). 2005;99(2):650–5.
18. Ream RS, Schreiner MS, Neff JD, McRae KM, Jawad AF, Scherer PW, Neufeld GR. Volumetric capnography in children. Influence of growth on the alveolar plateau slope. Anesthesiology. 1995;82(1):64–73.
19. Tsoukias NM, Tannous Z, Wilson AF, George SC. Single-exhalation profiles of NO and CO2 in humans: effect of dynamically changing flow rate. J Appl Physiol (1985). 1998;85(2):642–52.
20. Fowler WS. Lung function studies; the respiratory dead space. Am J Phys. 1948;154(3):405–16.
21. Bohr C. Über die Lungenatmung. Skan Arch Physiol. 1891;53:236–8.
22. H E. Volumen inefficax. Uppsala Laekareforen Forh. 1938;44:191–218.
23. Suarez-Sipmann F, Bohm SH, Tusman G. Volumetric capnography: the time has come. Curr Opin Crit Care. 2014;20(3):333–9.
24. Rodger MA, Bredeson CN, Jones G, Rasuli P, Raymond F, Clement AM, Karovitch A, Brunette H, Makropoulos D, Reardon M, et al. The bedside investigation of pulmonary embolism diagnosis study: a double-blind randomized controlled trial comparing combinations of 3 bedside tests vs ventilation-perfusion scan for the initial investigation of suspected pulmonary embolism. Arch Intern Med. 2006;166(2):181–7.
25. Bausell R, Li Y. Power analysis for experimental research: a practical guide for the biological, medical and social sciences. Cambridge: Cambridge University Press; 2002.
26. Lele EE, Hantos Z, Bitay M, Szivos B, Bogats G, Petak F, Babik B. Bronchoconstriction during alveolar hypocapnia and systemic hypercapnia in dogs with a cardiopulmonary bypass. Respir Physiol Neurobiol. 2011;175(1):140–5.
27. Kaczka DW, Brown RH, Mitzner W. Assessment of heterogeneous airway constriction in dogs: a structure-function analysis. J Appl Physiol (1985). 2009;106(2):520–30.

28. Fors D, Eiriksson K, Arvidsson D, Rubertsson S. Gas embolism during laparoscopic liver resection in a pig model: frequency and severity. Br J Anaesth. 2010;105(3):282–8.
29. Simon M, Battistini B, Joo Kim Y, Tsang J. Plasma levels of endothelin-1, big endothelin-1 and thromboxane following acute pulmonary air embolism. Respir Physiol Neurobiol. 2003;138(1):97–106.
30. Deem S, McKinney S, Polissar NL, Hedges RG, Swenson ER. Hemodilution during venous gas embolization improves gas exchange, without altering V(a)/Q or pulmonary blood flow distributions. Anesthesiology. 1999;91(6):1861–72.
31. Hedenstierna G, Sandhagen B. Assessing dead space. A meaningful variable? Minerva Anestesiol. 2006;72(6):521–8.
32. Elliott CG. Pulmonary physiology during pulmonary embolism. Chest. 1992;101(4 Suppl):163S–71S.
33. Hoellerich VL, Wigton RS. Diagnosing pulmonary embolism using clinical findings. Arch Intern Med. 1986;146(9):1699–704.
34. Petersson J, Glenny RW. Gas exchange and ventilation-perfusion relationships in the lung. Eur Respir J. 2014;44(4):1023–41.
35. Mondonedo JR, McNeil JS, Herrmann J, Simon BA, Kaczka DW. Targeted versus continuous delivery of volatile anesthetics during cholinergic bronchoconstriction. J Eng Sci Med Diagn Ther. 2018;1(3):031003–031001–031003-031010.
36. Siobal MS, Ong H, Valdes J, Tang J. Calculation of physiologic dead space: comparison of ventilator volumetric capnography to measurements by metabolic analyzer and volumetric CO2 monitor. Respir Care. 2013;58(7):1143–51.
37. Dos Santos RA, Fodor GH, Kassai M, Degrugilliers L, Bayat S, Petak F, Habre W. Physiologically variable ventilation reduces regional lung inflammation in a pediatric model of acute respiratory distress syndrome. Respir Res. 2020;21(1):288.
38. Porra L, Degrugilliers L, Broche L, Albu G, Strengell S, Suhonen H, Fodor GH, Petak F, Suortti P, Habre W, et al. Quantitative imaging of regional aerosol deposition, lung ventilation and morphology by synchrotron radiation CT. Sci Rep. 2018;8(1):3519.
39. Xu M, He H, Long Y. Lung perfusion assessment by bedside electrical impedance tomography in critically ill patients. Front Physiol. 2021;12:748724.
40. Edlinger-Stanger M, Bernardi MH, Kovacs K, Mascha M, Neugebauer T, Bohme S, Ayoubi N, Christofi N, Garry J, Fleming N, et al. The effect of acute ventilation-perfusion mismatch on respiratory heat exchange in a porcine model. PLoS One. 2021;16(7):e0254399.

Publisher's Note